Research Article | Vol. 29, No. 3 / 1 February 2021 / Optics Express 4091
Optics EXPRESS

Broad-band plasmonic isolator compatible with low-gyrotropy magneto-optical material

SEVAG ABADIAN,[1,3] GIOVANNI MAGNO,[1,2] VY YAM,[1] AND BEATRICE DAGENS[1,4]

[1] Université Paris-Saclay, Centre de Nanosciences et de Nanotechnologies, 91120 Palaiseau, France
[2] Dipartimento di Ingegneria Elettrica e dell'Informazione, Politecnico di Bari, Bari, Italy
[3] sevag.abadian@c2n.upsaclay.fr
[4] beatrice.dagens@c2n.upsaclay.fr

Abstract: Integration of optical isolators remains one the main technological issues of photonic circuits despite several decades of research. We propose a radically new concept which enables performing broad-band isolation even in the case of low-gyrotropy material, opening the road to a new class of non-reciprocal devices using easy-to-integrate composite materials. The principle explores the separation of back-and-forth light paths, induced by the coupled mode asymmetry in magnetoplasmonic slot waveguides. We show numerically that such a structure combined with suitable absorbers gives more than a 18 dB isolation ratio on several tens of nanometers bandwidth, with 2 dB insertion losses.

1. Introduction

The issue of the monolithic integration of optical isolators, and more generally of non-reciprocal devices in photonic circuits appeared with the rise of optical fiber telecommunications. Indeed, isolators are essential elements for the stability of laser diodes emission, and optical circulators can considerably enrich photonic circuits architecture. Their monolithic integration is the best solution to limit devices and circuits cost. Optical transmission non-reciprocity requires a propagation medium with together time and spatial symmetry breaking [1]. Over time, different mechanisms have been proposed, explored and improved to attain time-reversal breaking such as magneto-optics (MO) [2], optical nonlinear methods [3], dynamic modulation [4] or optomechanical interactions [5]. However, the most traditional way, and the most efficient one remains the use of magneto-optical effects. A first idea for integrated isolator was to reproduce the principle of bulk Faraday isolators [6,7], but the birefringence of the planar waveguides and the requirement for integrated polarizers prevent the realization of performing non-reciprocal devices. Only recently a promising alternative was proposed to integrate Faraday rotation isolators by using quasi-phase matched nonreciprocal mode conversion, mitigating the waveguide birefringence [8]. Nevertheless TMOKE (Transverse Magneto-Optical Effect) appears as the most compatible solution with planar rectangular waveguides: indeed, it is a reflection effect occurring at the MO material interface and it does not modify the light polarization. Additionally, integrated designs could be envisaged in standard photonic material systems with a MO layer as a top or side cladding. In this way two groups [9,10] simultaneously proposed to use transversely magnetized metallic MO cladding layers and exploit the imaginary part of the TMOKE, i.e., the non-reciprocal dichroic loss. Giving the whole structure an amplifying layout could compensate the remaining loss in the forward direction. The principle being inherently polarization dependent, non-reciprocal amplifier designs for TM mode [11,12] or for TE mode [13] were thus proposed and demonstrated for typically 12 dB isolation at transparency. In the meantime, Fujita et al used the phenomena of non-reciprocal phase shift (NRPS) induced by TMOKE. A new type of optical isolators in a TM mode configuration based on a garnet waveguide Mach Zehnder Interferometer (MZI) was demonstrated [14], and considerably improved since then [15]. An important aspect of

#415969 https://doi.org/10.1364/OE.415969
Journal © 2021 Received 24 Nov 2020; revised 16 Jan 2021; accepted 16 Jan 2021; published 25 Jan 2021

Optics EXPRESS

these types of isolators is that they face challenges such as complex integration on semiconductor platforms, they are much bigger in size compared to other structures and they operate at a narrow bandwidth. In search for isolators with better performance, reduced size and easier integrability, magnetic ring resonator structures have also been inspected. Since its first proposition in 2007 by N. Kono [16], several groups developed garnet oxide direct growth on semiconductor platforms [17,18], and/or highly resonant structures [19–21]. These structures can provide high isolation ratio and their miniaturized size facilitates integration with other optoelectronic devices, especially with semiconductor lasers. However, due to the nature of the ring resonator's sharp resonance, these isolators remain very sensitive to the geometrical parameters which limit their performance over a wide range of wavelengths. Alternative non-magneto-optical designs have also been proposed along these years based on different non-linearities [22–26], without improving MO garnet devices neither reducing operation budget nor footprint. MO garnet-based devices have undoubtedly led to the best device performance up to now. Nevertheless, garnet MZIs and ring resonators remain very narrow bandwidth solutions which cannot address all the applications.

In this paper, we propose a radically new guided isolator structure with respect to the mainstream of these last years. The principle of this new isolator is based on plasmonic slot waveguide modes which lose their symmetry by the use of a magnetized MO material inside the metal/dielectric/metal (MDM) slot. The phenomenon was identified a few years ago firstly in the case of anisotropic slot waveguide [27], and then more specifically in different magneto-plasmonic works [28,29]. More recently devices using this effect have been theoretically proposed for (reciprocal) switching in a plasmonic thin metallic waveguide [30] or modulation in a slot waveguide [31]. But no design was proposed for non-reciprocal devices.

Here we firstly detail the basic principle of the proposed guided isolator and we numerically evaluate its expected performance through relevant examples using "classical" MO material like Bismuth Iron Garnet (BIG) for operation around 1.55 μm. Then we derive an analytical model to understand the underlying physical mechanisms of the MO slot waveguide mode generation and to propose and generalize future designs compatible with fully integratable (low-gyrotropy) MO materials.

2. Isolator principle and specific design

Figure 1 depicts the proposed isolator operating at telecom wavelengths, which exploits a slot (MDM) waveguide whose core dielectric material has MO properties, e.g., BIG. The fundamental guided modes in the slot waveguide result from the coupling of two SPP (Surface Plasmon Polariton) modes which can exist simultaneously at each metal-dielectric interface. Their coupling generates two "supermodes", namely, the LRSPP (Long-Range-SPP) and SRSPP (Short-Range-SPP) modes, with respectively even and odd profiles of the electric field component. The magnetization of the MO material (directed along the y-axis) and the geometrical structure are so that each SPP undergoes TMOKE. Because of TMOKE, each supermode becomes asymmetric as schematized in Fig. 1(b) in the case of an Au-BIG-Au slot waveguide.

We call magneto-biplasmonic effect the result of TMOKE interaction in coupled plasmonic (SPP) modes. Whereas it has been considered up to now as usual magneto-plasmonic effect [31], we underline through this new name the fact that the two-step physical mechanism (mode coupling + TMOKE) radically modifies the impact of magneto-optics on guided mode propagation, as discussed later. By exciting only one of the supermodes (preferentially the low-losses LRSPP), light follows different paths in the forward and backward directions (time symmetry breaking), as shown in Fig. 1(b).

By introducing optical absorbers only on one side of the slot waveguide (spatial symmetry breaking), light is no more transmitted in the corresponding direction [Figs. 1(a), 1(b)]. Any kind of lossy element can be used, such as lossy cavities, with the condition that they do not induce any back reflections. Periodicity of these elements is not required either. As a result, isolation

Optics EXPRESS

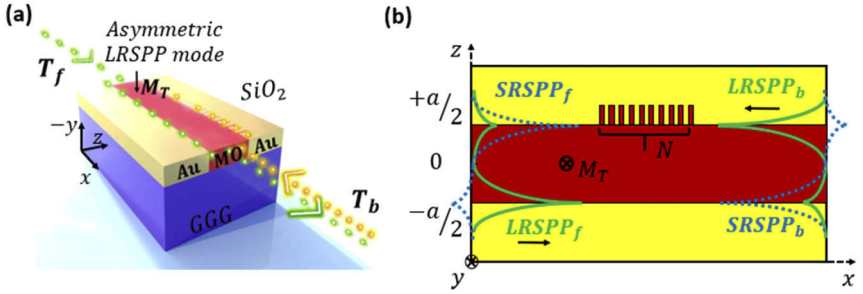

Fig. 1. (a) 3D schematic view of isolator. (b) Top view of the Au-BIG-Au waveguide, with N nanocavities positioned on one metal-dielectric interface. The BIG layer is magnetized along the y direction. Magnetic field profile H_y of the LRSPP mode (solid green) and of the SRSPP mode (dotted blue) are represented in forward (increasing x) and backward (decreasing x) senses.

ratio is controlled by two independent parameters: plasmonic coupled mode asymmetry and SPP absorption provided by the optical absorbers (lossy metallic cavities) for forward/backward transmission contrast.

In this part, we first numerically evaluate the asymmetry of the 2D waveguide modes of Fig. 1(b), before to study the lossy cavities' characteristics and finally the isolation performance of the full device. Finite Element Method (FEM) based calculations were performed using COMSOL Multiphysics 5.4, for a varying core width a, between 0.5 μm and 2.5 μm, and a varying incident wavelength λ_0, between 0.7 μm and 2.5 μm. An MDM structure thickness of $h = 0.45$ μm maximizes the optical confinement factor while maintaining vertical monomode behavior. The slot waveguide is placed on a GGG (Gallium Gadolinium Garnet) substrate with index $n_{GGG} = 1.97$ and covered with SiO_2 (Silica) cladding having an index $n_{SiO2} = 1.45$.

At optical frequencies, the MO activity in this configuration results in an optical anisotropy that can be described by the following dielectric tensor, being the magnetization $\overrightarrow{M_T} = M_T\overrightarrow{u_y}$:

$$\varepsilon = \begin{pmatrix} \varepsilon_{xx} & 0 & \varepsilon_{xz} \\ 0 & \varepsilon_{yy} & 0 \\ \varepsilon_{zx} & 0 & \varepsilon_{zz} \end{pmatrix}, \tag{1}$$

Having considered absorption zero ($\varepsilon'' = 0$), the diagonal elements ε_{xx}, ε_{yy}, ε_{zz} are equal to the scalar isotropic dielectric constant $\varepsilon_d = 2.3^2$. The off-diagonal elements are $\varepsilon_{xz} = -\varepsilon_{zx} = ig$ where g is the gyrotropy constant. $|g|$ is proportional to the magnitude of the saturation magnetization. In this part, we shall assume that g is a real constant equal to 0.01 [32] (corresponding to a Faraday rotation of $\theta_F = 5217°/\text{cm}$). The frequency ω dependent dielectric constant of gold is modeled by the Drude-Lorentz model fitting of ellipsometric data with plasma frequency $\omega_p = 1.29 \times 10^{16}\ rad/s$, plasma collision frequency $\gamma_c = 6.47 \times 10^{13}\ rad/s$ and $\varepsilon_\infty = 1$ the high-frequency contribution to the relative permittivity [33]:

$$\varepsilon_m(\omega) = \varepsilon_\infty - \frac{\omega_p^2}{\omega(i\gamma_c + \omega)}, \tag{2}$$

The mode asymmetry percentage is one of the key parameters of the isolator design: it should be maximized versus geometrical dimensions to optimize the isolation ratio. Two-dimensional modal analysis is performed on the proposed slot waveguide isolator to calculate LRSPP modes at the entrance of the device. The mode asymmetry is deduced from the absolute relative difference

Optics EXPRESS

of the magnetic field intensities at both metal-dielectric interfaces. As shown in the later sections of the paper and in the appendix, the mode asymmetry is a quantity which can be expressed as $\phi = 100 \times \left(1 - \left|\frac{H_y(z=-a/2)}{H_y(z=+a/2)}\right|\right)$.

As shown in Fig. 2, asymmetry is strongly dependent on geometry and on wavelength: for a fixed wavelength, the increasing width of the dielectric waveguide enhances the asymmetry of the LRSPP mode; besides, the asymmetry is also higher for lower wavelengths. These first data indicate that the isolation ratio could be geometrically controlled.

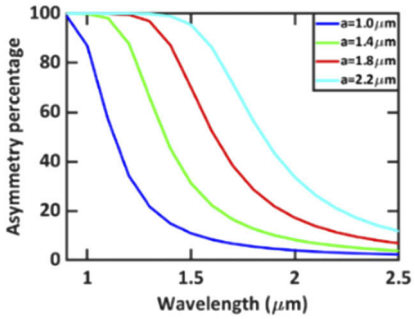

Fig. 2. Electromagnetic field asymmetry percentage in Au-BIG-Au slot waveguide versus the wavelength and for dielectric (BIG) widths a=1.0 μm, 1.4 μm, 1.8 μm and 2.2 μm for a fixed slot waveguide (BIG and Au) thickness h = 0.45 μm.

Furthermore, contrary to previously proposed TMOKE isolators, the propagating LRSPP mode in a MO MDM waveguide has identical effective indices in the forward and backward directions for waveguide symmetry reasons since the magnetization is applied along the y-axis; however light energy follows different paths (opposite interfaces of the MDM), and the one-side lossy nanocavities provide absorption on the backward signal. Although many complex nanocavity geometries could be considered, we suggest here elementary rectangular nanocavities as represented in Fig. 3, which are easy to integrate in the isolator structure with a manageable nano-fabrication process. The geometrical parameters of these recurrently placed nanocavities such as the length, l_{cav} (in the x direction) and width w_{cav} (in the z direction) can be properly and specifically designed to obtain the required optical response (high losses on a large bandwidth). Two other parameters which need to be addressed are the periodicity p_{cav} and the number of cavities N. Periodicity should be adequately chosen to avoid both the coupling between adjacent cavities and back reflections, whereas the number N should be as low as possible to decrease the total isolator length and minimize the plasmonic losses in the forward direction, and sufficiently high to provide complete absorption of the backward propagating light.

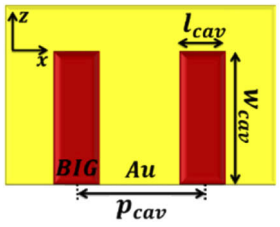

Fig. 3. Schematic of the lossy rectangular cavity formed by BIG and surrounded by Au.

The resonant condition of the rectangular nanocavity can be approximated by the Fabry-Perot (FP) equation [34]:

$$2m\pi = 2n_{eff,g(x,y)}k_0 w_{cav} + \varphi_{r1} + \varphi_{r3},\ m \in \mathbb{Z}, \tag{3}$$

Optics EXPRESS

where m is the order of the horizontal FP resonance and $n_{eff,g(x,y)}$ is the effective index of the fundamental mode within the BIG gap of the unitary cell calculated by considering a cross section parallel to the (x,y) plane. φ_{ri} is the reflection phase shift of the gap mode at each end of the cavity, with i=1 and i=3 corresponding to the reflection of light from the BIG waveguide and from the Au surrounding, respectively.

In Fig. 4, FDTD calculations give the absorption spectra for a fixed cavity length $l_{cav} = 0.1$ μm and different w_{cav}. From the FP equation it is quite evident that the increase in cavity width w_{cav} results in a redshift of a given FP resonance. Higher order horizontal FP resonant modes are also expected to appear as a result of this increase: for this reason, as w_{cav} grows the cavity absorption peak becomes sharper and stronger. Thus, a rectangular cavity with dimensions $l_{cav} = 0.1$ μm and $w_{cav} = 0.95$ μm can provide an absorption peak near $\lambda_0 = 1.55$ μm due to the fourth order horizontal Fabry Perot resonance happening inside the cavity as shown in the magnetic field plot of Fig. 4(e). Several cavities with these dimensions, integrated adjacent to each other on one interface of the MDM structure, are capable of absorbing the SPPs propagating on its side.

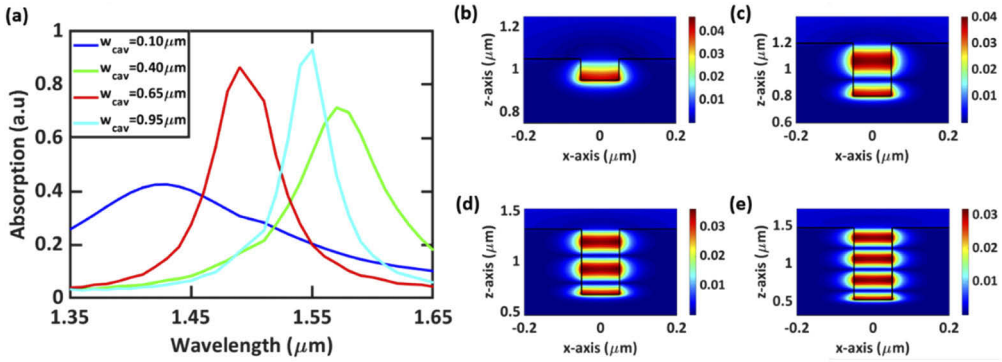

Fig. 4. Absorption spectra of a rectangular nanocavity as a function of λ_0 and w_{cav} for cavity length $w_{cav} = 0.10$ μm, 0.40 μm, 0.65 μm and 0.95 μm. (b-e) Intensity of the magnetic field along the (x,z) plane in increasing order presented in (a).

At this point, all the necessary components required to build a functioning isolator as shown in Fig. 1(a) have been discussed above. Using commercial software Lumerical based on FDTD method, 3D simulations have been performed in order to simulate the propagation of light in the forward and backward directions of the full structure. Isolation ratio, which is a quantitative measurement of the difference between the forward to the backward transmissions in dB, is defined as follows:

$$IR\ (dB) = 10\log_{10}(T^f / T^b), \tag{4}$$

Another relevant parameter is the Figure of Merit (FoM), which is the ratio of isolation to the insertion losses. FoM expresses the efficiency of the isolator structure and can be represented by the equation:

$$FoM = IR\ (dB)/10\log_{10}(T_f), \tag{5}$$

Here, T_f is the ratio of the power of the forward LRSPP mode at the output (port on the right end) divided by the power at the input (port on the left end). Similarly, T_b is the ratio of the power of the backward propagating LRSPP mode at the input (port on the left end) divided by the power at the output (port on the right end). Although visually both modes may seem different due to the inversion around the central axis z = 0 with the change in propagation direction, both forward and backward propagating modes are the LRSPP modes with identical phase profile and effective index. Thus, their respective transmission T_f and T_b can be compared to evaluate the isolation ratio.

Optics EXPRESS

In order to obtain optimum results for propagation simulations, a wide waveguide width a = 2.4 μm which promises a high asymmetry percentage is chosen to obtain the highest contrast between forward and backward transmissions in the wavelength range of 1.425 μm to 1.675 μm. In the coming results, rectangular cavities have dimensions l_{cav} = 0.1 μm and w_{cav} = 0.95 μm. Although the cavity arrangement is not of primary importance and randomly placed cavities can provide similar intended SPP absorption, we have positioned the ten cavities with a regular spacing p_{cav} = 0.8 μm, which is sufficient to avoid their mutual coupling and allows each cavity to absorb independently from the others.

In the forward direction the transmission curve takes a smooth shape [(black curve in Fig. 5(a)] while the majority of the LRSPP energy travel on one interface of the slot waveguide with very small interaction with the cavities as shown by the amplitude of the magnetic field surface plot in Fig. 6(a). Negligible backward reflections occur in this case [black curve in Fig. 5(b)]. On the other hand, the backward propagation of the LRSPP energy occurs on the interface with the periodically arranged nanocavities which provide absorption and induce a very perturbed and low transmission [red curve in Fig. 5(a)], this corresponds to the magnetic field plot of Fig. 6(b). In this sense of propagation some reflections occur due to the interaction of the SPP with the cavities [red curve in Fig. 5(b)].

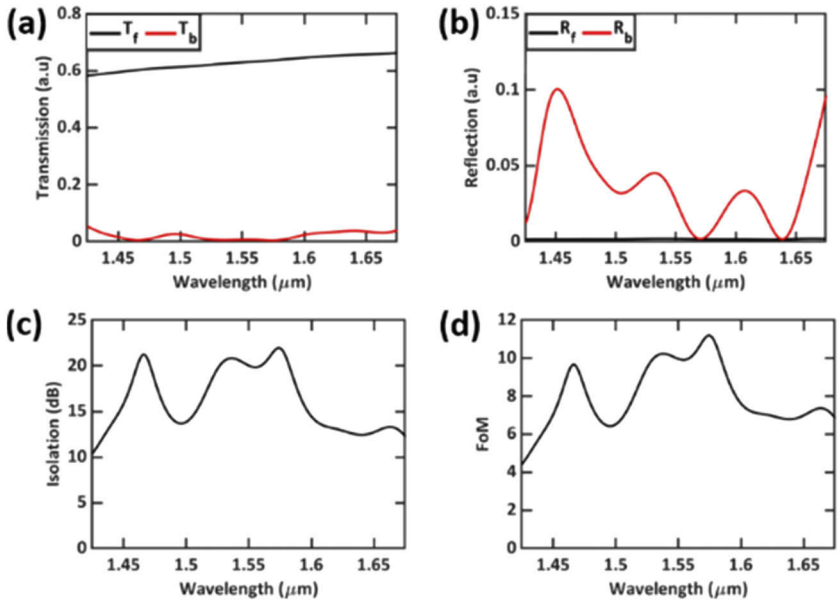

Fig. 5. (a) Forward and backward transmission (T_f, T_b) and (b) reflections (R_f, R_b). (c) Isolation ratio and (d) FoM for an isolator with width a = 2.4 μm, height h = 0.45 μm and total length of 11.2 μm.

These reflections have moderate impact on the isolator performance since they induce propagation in the increasing x direction. As we can notice in Figs. 5(c), 5(d) high isolation ratio and FoM are obtained over the wavelength range of interest which are due to i) the high asymmetry percentage of the coupled LRSPP mode hosted by the magnetized MO slot waveguide, and ii) the losses due to horizontal FP resonances of the rectangular cavities. Notably, isolation ratio higher than 18 dB and FoM higher than 9 are obtained between wavelengths 1.52 μm and 1.58 μm, with the highest value of isolation ratio reaching 22 dB and FoM 11 around λ_0 = 1.57 μm.

Optics EXPRESS

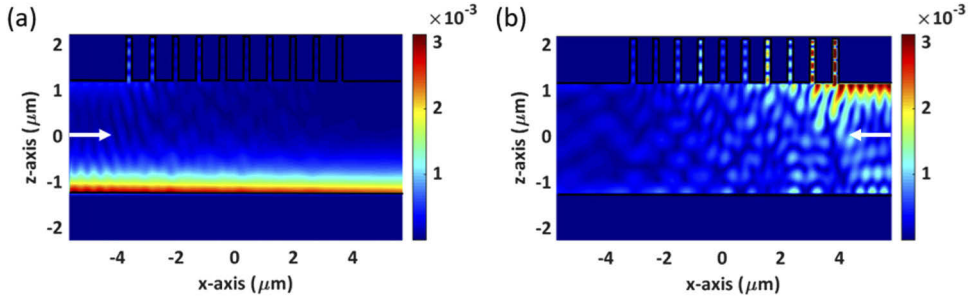

Fig. 6. Intensity of magnetic field along the (x,z) plane (top view of the device), when y = 0 μm and λ_0 = 1.57 μm, for (a) forward and (b) backward transmission directions respectively, in the case of isolator width a = 2.4 μm, height h = 0.45 μm and total length of 11.2 μm.

The simple design we proposed (consisting of a single linear array of absorbing cavities) already shows the potential of this non-reciprocal structure. It is worth underlining that the different degrees of freedom shown by the structure enable a high isolation value with both low back reflections and high FoM values over a large spectral range.

3. Analytical derivation toward low gyrotropy material

The following analytical framework is developed in order to deepen the physical understanding of the magneto-biplasmonics effect in MO slot waveguides and to identify design optimization rules especially in the case of more integratable low-gyrotropy MO materials. We start our study by deriving an analytical model based on Maxwell's equations applied to the magneto-optical MDM structure shown in Fig. 1(b). A semi-vectorial approximation is used in order to simplify the analytical work, where instead of the six electromagnetic fields, the (coupled) SPP modes in the slot waveguide are considered to be composed of the three largest non-zero field components E_x, H_y and E_z, where x is the propagation direction, y the magnetization direction, and z the transverse direction. These electromagnetic fields have a maximum value at each dielectric-metal interfaces and exponentially decay in both the metal and the dielectric material. By using Maxwell's equations in magneto-optical media, i.e., considering the MO dielectric tensor including off-diagonal elements as shown in Eq. (1), the wave equation and the relation between the electromagnetic fields can be derived. The solutions for the magnetic field y-component Hy that satisfy the H-field boundary conditions at z = ± a/2, where a, is the width of the dielectric region inside the MDM, can be written as:

$$e^{i\beta x}\begin{cases} Ae^{-k_m(z-a/2)}, & z \geq +a/2 \\ Ce^{k_d(z-a/2)} + De^{-k_d(z+a/2)}, & -a/2 \leq z \leq +a/2 \\ Be^{k_m(z+a/2)}, & z \leq -a/2 \end{cases}, \tag{6}$$

where k_m and k_d are the wavevectors z-components in the metal and dielectric layers respectively and β is the propagation constant of the traveling wave in the x direction.

The dispersion relation of the optical modes supported by the MDM structure, with MO material having the diagonal element of the dielectric tensor $\varepsilon_d = n_{MO}^2$, can be derived by applying the boundary conditions on the tangential electromagnetic fields at the metal-dielectric interfaces [Eq. (6)]:

$$e^{-2k_d a} = \frac{\left(\beta\gamma_{xz}^d\right)^2 + \left(k_d\gamma_{xx}^d + k_m\gamma_{xx}^m\right)^2}{\left(\beta\gamma_{xz}^d\right)^2 + \left(k_d\gamma_{xx}^d - k_m\gamma_{xx}^m\right)^2}, \tag{7}$$

Optics EXPRESS

where $\gamma_{xz}^{d} = ig/(n_{MO}^4 - g^2)$, $\gamma_{xx}^{d} = n_{MO}^2/(n_{MO}^4 - g^2)$, $\gamma_{xx}^{m} = 1/n_{Au}^2$ and the wavevectors k_m and k_d can be represented by $k_i = \sqrt{\beta^2 - k_0^2/\gamma_{xx}^{i}}$, $i = m, d$ and $k_0 = 2\pi/\lambda_0$, k_0 being the wavenumber in free space and λ_0 the operating optical wavelength.

By considering $g^2 \ll n_{MO}^4$ and $\varepsilon_m - \varepsilon_d \cong \varepsilon_m$ the complex propagation constant β of the MDM waveguide plasmonic modes, LRSPP and SRSPP, can be formalized and expressed in a comprehensible way:

$$\beta \approx \beta_0 \pm \sqrt{\beta_g^2 + \beta_a^2}, \tag{8}$$

where $\beta_g = \frac{\beta_0 g}{(1-\varepsilon_d^2/\varepsilon_m^2)\sqrt{-\varepsilon_d\varepsilon_m}}$, $\beta_a = \frac{2\beta_0 e^{-k_d a}}{(1-\varepsilon_d^2/\varepsilon_m^2)}\left(\frac{-\varepsilon_d}{\varepsilon_m}\right)$ and $\beta_0 = k_0\sqrt{\frac{\varepsilon_m\varepsilon_d}{\varepsilon_m+\varepsilon_d}}$ is the wavenumber of an SPP on a single metal-dielectric interface without magnetization. The "plus" and "minus" signs in Eq. (8) correspond respectively to the LRSPP and SRSPP modes.

β_g and β_a can be seen as modifications to the single SPP propagation constant β_0. These two terms are respectively related to the gyrotropy and to the SPP modes coupling (strength and overlap) of the magneto-optical slot waveguide. If an infinite thickness a is considered (which corresponds to $\beta_a \approx 0$), Eq. (8) gives the expression of the single MO SPP propagation constants, depending on the considered interface (or equivalently on propagation direction, or on g sign [35]). On the contrary if g = 0 ($\beta_g \approx 0$), the same equation reduces to the canonical non-MO LRSPP and SRSPP propagation constants. For application purposes, it is much more convenient to consider the LRSPP mode only because of lower propagation losses with respect to the SRSPP mode.

It is worth noting that the dispersion relation represented in Eq. (7) is reciprocal since it depends on the square of the propagation constant β^2. Thus, the numerical variation observed in β (or as a result in the mode effective index n_{eff}) is dependent solely on gyrotropy absolute value $|g|$, on slot width a and on material permittivities, but not on the propagation direction.

In the non-magnetic case ($\beta_g = 0$) the amplitude of the magnetic field H_y is the same at the two dielectric-metal interfaces ($A = B$). However, and upon the presence of magnetization in the y direction (time symmetry breaking) in the sandwiched dielectric layer, the electromagnetic field distribution is altered and the SPP amplitude at the two dielectric-metal interfaces are no longer identical: $A \neq B$. In order to quantify the degree of the mode asymmetry, the parameter ϕ is defined as the percentage of the normalized absolute difference between the amplitude of the magnetic field at z = +a/2 and at z = -a/2. ϕ can be deduced using Eqs. (6) and (7).

$$\phi = 100 \times \left(1 - \left|\frac{H_y(z=-a/2)}{H_y(z=+a/2)}\right|\right) = 100 \times \left(1 - \left|\sqrt{\frac{1-\alpha}{1+\alpha}}\right|\right), \tag{9}$$

where $\alpha = g/(2e^{-k_d a}\varepsilon_d^{3/2}/\sqrt{-\varepsilon_m})$

As it can be seen from the derived Eq. (9) and the complex expression of α, the quantity ϕ is in direct relation with the gyrotropy of the magneto-optical material g, the waveguide width a and the incident wavelength λ_0. For a given metal and at a fixed wavelength, the width a and the permittivity (diagonal element) of the magneto-optical layer have the strongest influence on the mode asymmetry, since they both contribute to the exponential term. For our application, both the width and the MO material dielectric constant should thus be increased, in the limit of the existence of the coupled LRSPP mode. This limit can be assessed by the mode losses which are lower for LRSPP mode than the uncoupled SPP one.

The derived analytical model can be used now to evaluate design rules and expected performance in term of mode asymmetry. To first check the validity of this approximated model in Fig. 7, we have calculated the degree of mode asymmetry ϕ by using the analytical model and COMSOL, in the case of two values of gyrotropy (0.1 and 0.01), for arbitrary theoretical dielectric material permittivities (diagonal element). The overall tendency is well reproduced by the analytical

Optics EXPRESS

model, although the use of the semi-vectorial approximation may introduce a relative error of ± 0.3% on the asymmetry percentage of the LRSPP mode [36].

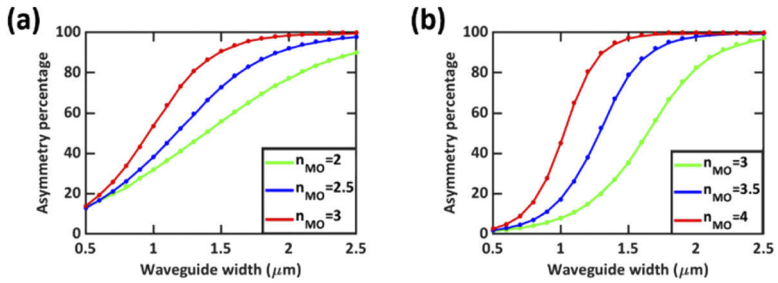

Fig. 7. (1D case) Magnetic field asymmetry percentage for gyrotropy (a) g = 0.1, and n_{MO}=2, 2.5 and 3; (b), g = 0.01 and n_{MO}=3, 3.5 and 4; for a fixed incident wavelength λ_0=1.55 μm and waveguide width ranging between 0.5 μm and 2.5 μm . Straight lines represent results obtained from modal study using COMSOL Multiphysics whereas the asterisks represent results from analytical model.

According to Figs. 7(a), 7(b) the decrease in asymmetry due to the decrease in gyrotropy can be compensated by the increase in the refractive index of the magneto-optical dielectric. Nevertheless, the impact of refractive index is more strongly marked when gyrotropy is low. For a 2 μm waveguide width and an optical index equal to 3, the asymmetry of the LRSPP mode can reach more than 95% in the case of very high gyrotropy g = 0.1 (corresponding to a Faraday rotation of θ_F = 52174°/cm), and more than 80% in the case of the more realistic value g=0.01.

We can also consider a new class of composite MO materials with gyrotropy as low as g = 0.005 (corresponding to a Faraday rotation of θ_F = 2609°/cm) which have been recently demonstrated [37]. In such a composite material the refractive index can be managed partly independently of the MO properties. Even if the gyrotropy is quite low in such a diluted material, the effect on asymmetry of the coupled mode can be compensated by the effective index. In this context we have considered in Fig. 8 the expected asymmetry induced in magneto-biplasmonic waveguides with different refractive indices, in the case of g = 0.005.

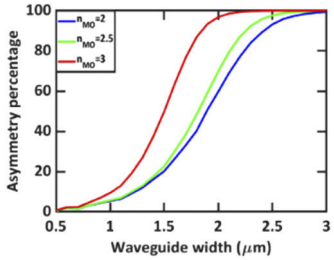

Fig. 8. (2D case) Electromagnetic field asymmetry percentage in Au-BIG-Au slot waveguide for gyrotropy g = 0.005, and a variation of the dielectric refractive index nMO = 2, 2.5 and 3, for a fixed incident wavelength λ0 = 1.55 μm, waveguide width 1.2 μm and thickness h = 0.45 μm.

Promising results show asymmetry higher than 95% with realistic integratable MO material ($2 < n_{MO} < 2.5$). In all the cases, the simplest parameter to tune remains the waveguide width [38].

Optics EXPRESS

4. Discussion

We have shown through specific examples the potential of magneto-biplasmonics for optical isolators. Nevertheless, the analytical model can be further analyzed in order to show that this concept is quite general. Indeed, Eq. (8) gives similar expressions as the eigenvalues obtained with the Improved Coupled-Mode Theory [39] in the case of the coupling of two different waveguides: the both coupled waveguides would be here the interfaces supporting the SPPs, their "difference" being induced by the gyrotropy (via TMOKE), and their coupling factor would be related to the SPP penetration into the dielectric waveguide, included in the term $e^{-k_d a}$. Additionally it appears that α [in Eq. (9)] is equal to the ratio β_g/β_a, i.e., the asynchronism factor of the coupled modes as defined in Ref. [39]. This asynchronism factor represents the competitive contribution to the coupled mode asymmetrisation, of the both SPPs 'difference' (indicated by β_g which favours the asymmetrisation) and of their coupling strength and/or overlap (indicated by β_a which counteracts it). The plasmonic nature of the both coupled 'waveguides' (interfaces) makes here the asynchronism factor very sensitive to geometrical parameters: indeed the mode coupling decreases rapidly with the increase of slot waveguide width whereas the optical intensity remains concentrated at the MO-metal interface where TMOKE occurs. Asymmetry increases thus with width a. Also, for this reason, higher asymmetry is obtained for lower wavelengths, at which more confined SPP can be obtained as well for gold (Fig. 2) as for silver slot waveguides. Additionally, the light concentration at the plasmonic interfaces is also enhanced by the dielectric permittivity which has strong impact on mode profile through the term $e^{-k_d a}$. We expect similar asymmetry of the supermodes in coupled MO all-dielectric waveguides system, without the advantage of the light concentration and of the TMOKE enhancement induced by plasmonic effect. Magneto-biplasmonics provides thus a technological breakthrough in the integrated non-reciprocal devices domain, which could be combined with magneto-biphotonic (non-metallic) structures for lower insertion losses.

Besides, the next step will be the implementation of this new isolator structure in a photonic circuit. Whereas such integration has not yet been optimized, a possible full structure could use a mode converter for the transition from a fundamental mode hosted by a standard dielectric waveguide to the plasmonic mode confined in the MDM slot waveguide, similarly to what has been proposed in [40]. Impedance (effective index) matching technique can be used to design a high efficiency coupler to preferentially excite the LRSPP mode with low back reflections [41].

5. Conclusion

For decades, the performance of integrated photonic isolators was limited by integration issues, high insertion losses or low operation bandwidth. Here we propose a novel isolator principle which has the potential to tackle simultaneously these three previous issues. Based on the "magneto-biplasmonic" effect which occurs in MO slot waveguide, the proposed isolator can reach typically 20 dB isolation ratio with less than 2 dB insertion losses and on several nm bandwidth, by using low-gyrotropy (<0.005) MO material. In addition to a versatile design, adaptable for different wavelength ranges, the structure allows thus for example the use of MO composite material, easy to integrate on any photonic platform by sol-gel process.

The remaining step will be to design the interface of the proposed isolator with photonic circuits, which can be performed by usual device engineering of impedance matching, in order to excite solely the asymmetric LRSPP mode of the slot waveguide with minor back reflections and in a short propagation distance.

The potentiality of the proposed concept is assessed by the analysis of the mechanisms underlying the "magneto-biplasmonic" effect, which can be enhanced thanks to several design degrees of freedom, including geometrical parameters. The previous limitation in MO devices, mainly due to the low-gyrotropy of MO materials, is compensated by 'easy to control' geometrical

Optics EXPRESS

parameters in MO-biplasmonics: this opens the road to highly performing integrated non-reciprocal devices, and also many other photonic functions like switches or modulators.

6. Method

Finite Element Method (FEM) based calculations were performed using COMSOL Multiphysics 5.4 including the Electromagnetic Waves Frequency Domain module (emw) physics interface. The COMSOL simulation area is composed of a three-layer heterostructure identical to the MDM geometry represented in Fig. 1(a). Extremely fine triangular mesh is used, with largest element size ~a/100, at the dielectric-metal boundaries to give reliable and persistent results. The structure is excited from the left with a Numeric port, while scattering boundary condition is applied on the other boundaries of the structure to eliminate any back reflections that could alter the results. Using boundary mode analysis for the input port, the properties of interest of the 1D MDM waveguide can be retrieved. Similarly, the properties of the 2D slot waveguide interface are obtained using modal analysis. Finally, to evaluate the mode asymmetry percentage, operators are assigned on each of the metal-dielectric interfaces to collect the electromagnetic field intensity.

Using the commercial software Lumerical FDTD Solutions two simulation tasks are performed. In the FDTD method, a spatial discretization mesh of size $\Delta x = \Delta y = 10$ nm is imposed on the structure which is found enough for convergence of the numerical results. First, in order to study the optical response of the unitary cell with respect to the w_{cav} and l_{cav}, 2D simulations have been performed. A plane wave source with a frequency monitor are included in the simulation region and placed above the nanocavity to excite and record the intensity of absorption, respectively. Finally, to evaluate the performance of the isolator design, 3D simulations are launched, and the structure is excited using ports, which can simultaneously act as an exciting source for the required mode and a frequency monitor to collect transmission and reflection coefficients.

Appendix

The magnetic field components in the considered trilayer can be written in the form:

$$H_y = e^{i\beta x}\begin{cases} Ae^{-k_m(z-a/2)} & z \geq a/2 \\ Ce^{k_d(z-a/2)} + De^{-k_d(z+a/2)} & -a/2 \leq z \leq a/2 \\ Be^{k_m(z+a/2)} & z \leq -a/2 \end{cases}, \tag{10}$$

where k_m and k_d are the wavevectors z-components in the metal and dielectric layers, respectively. β is the propagation constant of the traveling wave in the x direction. Applying the continuity of the electromagnetic fields, at the opposing boundaries $z = a/2$ and $z = -a/2$ for this wave, we find:

$$A = C + D\exp(-k_d a), \tag{A.2}$$

$$B = C\exp(-k_d a) + D, \tag{A.3}$$

$$C = D\exp(-k_d a)\frac{\beta\gamma_{xz}^d + i(k_d\gamma_{xx}^d - k_m\gamma_{xx}^m)}{-\beta\gamma_{xz}^d + i(k_d\gamma_{xx}^d + k_m\gamma_{xx}^m)}, \tag{11}$$

The dispersion relation of the optical modes supported by the MDM structure, with MO material having the diagonal element of the dielectric tensor $\varepsilon_d = n_{MO}^2$, can be derived by applying the

Optics EXPRESS

boundary conditions on the tangential electromagnetic fields at the metal-dielectric interfaces.

$$e^{-2k_d a} = \frac{\left(\beta\gamma_{xz}^d\right)^2 + \left(k_d\gamma_{xx}^d + k_m\gamma_{xx}^m\right)^2}{\left(\beta\gamma_{xz}^d\right)^2 + \left(k_d\gamma_{xx}^d - k_m\gamma_{xx}^m\right)^2}, \tag{12}$$

By examining each term, we notice that this transcendental equation depends only on the square of the propagation constant β. Thus, the dispersion relation is reciprocal. As a result, the propagation constants for the modes propagating in the positive and negative x direction are the same, i.e., the solution of the dispersion relation does not change when propagation direction is reversed from β to −β.

Expanding and replacing the terms γ_{xx}^d, γ_{zx}^d and γ_{xx}^m by $\frac{\varepsilon_d}{\varepsilon_d^2-g^2}$, $\frac{ig}{\varepsilon_d^2-g^2}$ and $\frac{1}{\varepsilon_m}$ respectively, the dispersion relation can be rearranged to:

$$e^{-2k_d a} = \frac{\left[\frac{k_m}{\varepsilon_m} + \frac{1}{\varepsilon_d^2-g^2}(-\beta g + k_d\varepsilon_d)\right]\left[\frac{k_m}{\varepsilon_m} + \frac{1}{\varepsilon_d^2-g^2}(\beta g + k_d\varepsilon_d)\right]}{\left[\frac{k_m}{\varepsilon_m} - \frac{1}{\varepsilon_d^2-g^2}(\beta g + k_d\varepsilon_d)\right]\left[\frac{k_m}{\varepsilon_m} - \frac{1}{\varepsilon_d^2-g^2}(-\beta g + k_d\varepsilon_d)\right]}, \tag{13}$$

To decrease the apparent complexity and make the dispersion relation more appealing to the reader, the following substitutions are advised: $q_m = \frac{k_m}{\varepsilon_m}$, $q_g = \frac{1}{\varepsilon_d^2-g^2}(\beta g + k_d\varepsilon_d)$ and $q_{-g} = \frac{1}{\varepsilon_d^2-g^2}(-\beta g + k_d\varepsilon_d)$.

$$e^{-2k_d a} = \frac{[q_m + q_g][q_m + q_{-g}]}{[q_m - q_g][q_m - q_{-g}]}, \tag{14}$$

Upon the presence of magnetization in the y direction in the sandwiched dielectric layer, the electromagnetic field distribution is altered and the SPP amplitude at the two dielectric-metal interfaces are no longer identical ($A \neq B$). In order to quantify the degree of the mode asymmetry, the parameter ϕ is defined as the percentage of the normalized absolute difference between the amplitude of the magnetic field at $z = +a/2$ and at $z = -a/2$. It is normalized with respect to the maximum magnetic field amplitude, thus here:

$$\phi = 100 \times \left(1 - \left|\frac{H_y(z=-a/2)}{H_y(z=+a/2)}\right|\right) = 100 \times \left(1 - \left|\frac{B}{A}\right|\right), \tag{15}$$

Utilizing the expressions of A and B, and the dispersion relation in Eq. (14) one can rewrite the expression of asymmetry in the following way.

$$\phi = 100 \times \left(1 - \left[\frac{[q_m - q_g][q_m + q_{-g}]}{[q_m + q_g][q_m - q_{-g}]}\right]^{\frac{1}{2}}\right), \tag{16}$$

Replacing q_m, q_g and q_{-g} by their expressions can reduce the expression under the radical

$$\left[\frac{[q_m - q_g][q_m + q_{-g}]}{[q_m + q_g][q_m - q_{-g}]}\right]^{\frac{1}{2}} = \left[\frac{1 - \frac{b\beta\sqrt{\beta^2-c}}{w\beta^2+d}}{1 + \frac{b\beta\sqrt{\beta^2-c}}{w\beta^2+d}}\right]^{\frac{1}{2}} = \left[\frac{1-\alpha}{1+\alpha}\right]^{\frac{1}{2}}, \tag{17}$$

where $w = \frac{1}{\varepsilon_m^2} - \frac{\varepsilon_d^2}{(\varepsilon_d^2-g^2)^2} + \frac{g^2}{(\varepsilon_d^2-g^2)^2}$, $b = \frac{2g}{\varepsilon_m(\varepsilon_d^2-g^2)}$, $c = \varepsilon_m k_0^2$ and $d = -\frac{1}{\varepsilon_m} + \frac{\varepsilon_d}{\varepsilon_d^2-g^2}$

$$\alpha = \frac{b\beta\sqrt{\beta^2 - c}}{w\beta^2 + d}, \tag{18}$$

For high gyrotropy g=0.1, it is preferential to use the expression presented in Eq. (18) for α. Whereas, for lower gyrotropy values, we can follow minor assumptions like $\varepsilon_d^2 - g^2 \approx \varepsilon_d^2$, and

Optics EXPRESS

$Re(\varepsilon_m) \gg \varepsilon_d$, α can be simplified further and written as

$$\alpha = g/(2\exp(-k_d a)\varepsilon_d^{3/2}/\sqrt{-\varepsilon_m}), \tag{19}$$

Thus, we can see more clearly the dependence of this quantity and eventually the asymmetry percentage ϕ on the gyrotropy of the magneto-optical material g, the waveguide width and incident wavelength λ_0.

Acknowledgments. GM acknowledges the program "Research for Innovation" POR Puglia FESR FSE 2014-2020.

Disclosures. The authors declare no conflicts of interest.

References

1. D. Jalas, A. Petrov, M. Eich, W. Freude, S. Fan, Z. Yu, R. Baets, M. Popović, A. Melloni, J. D. Joannopoulos, M. Vanwolleghem, C. R. Doerr, and H. Renner, "What is-and what is not-an optical isolator," Nat. Photonics **7**(8), 579–582 (2013).
2. T. Rasing, "Nonlinear magneto-optics," J. Magn. Magn. Mater. **175**(1-2), 35–50 (1997).
3. M. Trzeciecki and W. Hübner, "Time-reversal symmetry in nonlinear optics," Phys. Rev. B: Condens. Matter Mater. Phys. **62**(21), 13888–13891 (2000).
4. I. A. D. Williamson, M. Minkov, A. Dutt, J. Wang, A. Y. Song, and S. Fan, "Breaking Reciprocity in Integrated Photonic Devices Through Dynamic Modulation," ACS Photonics **7**(7), 1729–1741 (2020).
5. X. Y. Lü, H. Jing, J. Y. Ma, and Y. Wu, "PT -Symmetry-Breaking Chaos in Optomechanics," Phys. Rev. Lett. **114**(25), 253601 (2015).
6. R. Wolfe, J. F. Dillon, R. A. Lieberman, and V. J. Fratello, "Broadband magneto-optic waveguide isolator," Appl. Phys. Lett. **57**(10), 960–962 (1990).
7. R. Wolfe, V. J. Fratello, and M. McGlashan-Powell, "Thin-film garnet materials with zero linear birefringence for magneto-optic waveguide devices (invited)," J. Appl. Phys. **63**(8), 3099–3103 (1988).
8. K. Srinivasan, C. Zhang, P. Dulal, C. Radu, T. E. Gage, D. C. Hutchings, and B. J. H. Stadler, "High-Gyrotropy Seedlayer-Free Ce:TbIG for Monolithic Laser-Matched SOI Optical Isolators," ACS Photonics **6**(10), 2455–2461 (2019).
9. M. Takenaka and Y. Nakano, "Proposal of a novel semiconductor optical waveguide isolator," *Conference Proceedings - International Conference on Indium Phosphide and Related Materials* 289–292 (1999).
10. W. Zaets and K. Ando, "Optical waveguide isolator based on nonreciprocal loss/gain of amplifier covered by ferromagnetic layer," IEEE Photonics Technol. Lett. **11**(8), 1012–1014 (1999).
11. W. V. Parys, B. Moeyersoon, D. V. Thourhout, R. Baets, M. Vanwolleghem, B. Dagens, J. Decobert, O. L. Gouezigou, D. Make, R. Vanheertum, and L. Lagae, "Transverse magnetic mode nonreciprocal propagation in an amplifying AlGaInAs/InP optical waveguide isolator," Appl. Phys. Lett. **88**(7), 071115 (2006).
12. M. Vanwolleghem, W. V. Parys, D. V. Thourhout, R. Baets, F. Lelarge, O. Gauthier-Lafaye, B. Thedrez, R. Wirix-Speetjens, and L. Lagae, "Experimental demonstration of nonreciprocal amplified spontaneous emission in a CoFe clad semiconductor optical amplifier for use as an integrated optical isolator," Appl. Phys. Lett. **85**(18), 3980–3982 (2004).
13. H. Shimizu and Y. Nakano, "Fabrication and characterization of an InGaAsp/InP active waveguide optical isolator with 14.7 dB/mm TE mode nonreciprocal attenuation," J. Lightwave Technol. **24**(1), 38–43 (2006).
14. J. Fujita, M. Levy, R. M. Osgood, L. Wilkens, and H. Dötsch, "Waveguide optical isolator based on Mach-Zehnder interferometer," Appl. Phys. Lett. **76**(16), 2158–2160 (2000).
15. Y. Shoji and T. Mizumoto, "Magneto-optical non-reciprocal devices in silicon photonics," Sci. Technol. Adv. Mater. **15**(1), 014602 (2014).
16. N. Kono, K. Kakihara, K. Saitoh, and M. Koshiba, "Nonreciprocal microresonators for the miniaturization of optical waveguide isolators," Opt. Express **15**(12), 7737 (2007).
17. L. Bi, J. Hu, P. Jiang, D. H. Kim, G. F. Dionne, L. C. Kimerling, and C. A. Ross, "On-chip optical isolation in monolithically integrated non-reciprocal optical resonators," Nat. Photonics **5**(12), 758–762 (2011).
18. B. J. H. Stadler and T. Mizumoto, "Integrated magneto-optical materials and isolators: A review," IEEE Photonics J. **6**(1), 1–15 (2014).
19. M.-C. Tien, T. Mizumoto, P. Pintus, H. Kromer, and J. E. Bowers, "Silicon ring isolators with bonded nonreciprocal magneto-optic garnets," Opt. Express **19**(12), 11740 (2011).
20. P. Pintus, D. Huang, C. Zhang, Y. Shoji, T. Mizumoto, and J. E. Bowers, "Microring-Based Optical Isolator and Circulator with Integrated Electromagnet for Silicon Photonics," J. Lightwave Technol. **35**(8), 1429–1437 (2017).
21. P. Pintus, D. Huang, P. A. Morton, Y. Shoji, T. Mizumoto, and J. E. Bowers, "Broadband TE Optical Isolators and Circulators in Silicon Photonics Through Ce:YIG Bonding," J. Lightwave Technol. **37**(5), 1463–1473 (2019).
22. Z. Yu and S. Fan, "Complete optical isolation created by indirect interband photonic transitions," Nat. Photonics **3**(2), 91–94 (2009).
23. D. Pile, Z. Yu, and S. Fan, "Optical isolation: A non-magnetic approach," Nat. Photonics **5**(9), 517 (2011).
24. C. R. Doerr, N. Dupuis, and L. Zhang, "Optical isolator using two tandem phase modulators," Opt. Lett. **36**(21), 4293 (2011).

Optics EXPRESS

25. F. Ruesink, M. A. Miri, A. Alù, and E. Verhagen, "Nonreciprocity and magnetic-free isolation based on optomechanical interactions," Nat. Commun. **7**(1), 13662 (2016).
26. L. D. Tzuang, K. Fang, P. Nussenzveig, S. Fan, and M. Lipson, "Non-reciprocal phase shift induced by an effective magnetic flux for light," Nat. Photonics **8**(9), 701–705 (2014).
27. I. D. Rukhlenko, M. Premaratne, and G. P. Agrawal, "Guided plasmonic modes of anisotropic slot waveguides," Nanotechnology **23**(44), 444006 (2012).
28. E. Ferreiro-Vila, J. M. García-Martín, A. Cebollada, G. Armelles, and M. U. González, "Magnetic modulation of surface plasmon modes in magnetoplasmonic metal-insulator-metal cavities," Opt. Express **21**(4), 4917 (2013).
29. D. Nikolova and A. J. Fisher, "Switching and propagation of magnetoplasmon polaritons in magnetic slot waveguides and cavities," Phys. Rev. B: Condens. Matter Mater. Phys. **88**(12), 125136 (2013).
30. K. S. Ho, S. J. Im, J. S. Pae, C. S. Ri, Y. H. Han, and J. Herrmann, "Switchable plasmonic routers controlled by external magnetic fields by using magneto-plasmonic waveguides," Sci. Rep. **8**(1), 1–8 (2018).
31. A. Haddadpour, V. F. Nezhad, Z. Yu, and G. Veronis, "Highly compact magneto-optical switches for metal-dielectric-metal plasmonic waveguides," Opt. Lett. **41**(18), 4340 (2016).
32. E. Popova, L. Magdenko, H. Niedoba, M. Deb, B. Dagens, B. Berini, M. Vanwolleghem, C. Vilar, F. Gendron, A. Fouchet, J. Scola, Y. Dumont, M. Guyot, and N. Keller, "Magnetic properties of the magnetophotonic crystal based on bismuth iron garnet," J. Appl. Phys. **112**(9), 093910 (2012).
33. G. Magno, M. Fevrier, P. Gogol, A. Aassime, A. Bondi, R. Mégy, and B. Dagens, "Strong coupling and vortexes assisted slow light in plasmonic chain-SOI waveguide systems," Sci. Rep. **7**(1), 7228 (2017).
34. Y. Ding, J. Yoon, M. H. Javed, S. H. Song, and R. Magnusson, "Mapping surface-plasmon polaritons and cavity modes in extraordinary optical transmission," IEEE Photonics J. **3**(3), 365–374 (2011).
35. V. I. Belotelov, I. A. Akimov, M. Pohl, V. A. Kotov, S. Kasture, A. S. Vengurlekar, A. V. Gopal, D. R. Yakovlev, A. K. Zvezdin, and M. Bayer, "Enhanced magneto-optical effects in magnetoplasmonic crystals," Nat. Nanotechnol. **6**(6), 370–376 (2011).
36. P. Pintus, "Accurate vectorial finite element mode solver for magneto-optic and anisotropic waveguides," Opt. Express **22**(13), 15737 (2014).
37. L. Bsawmaii, E. Gamet, F. Royer, S. Neveu, and D. Jamon, "Longitudinal magneto-optical effect enhancement with high transmission through a 1D all-dielectric resonant guided mode grating," Opt. Express **28**(6), 8436 (2020).
38. A. Haddadpour, V. Foroughi Nezhad, Z. Yu, and G. Veronis, "Magneto-optical switches in metal-dielectric-metal plasmonic waveguides," Proc. SPIE **9546**, 95461S (2015).
39. S. Lien and C. Ng, *Physics of Optoelectronic Devices* (Wiley Series in Pure and Applied Optics, 1995).
40. A.A. Kashi, J.J.G.M. van der Tol, Y. Jiao, and K. Williams, "Development of plasmonic slot waveguide on InP membrane," *23rd Annual Symposium of the IEEE Photonics Benelux Chapter*, Brussels, Belgium, 2018.
41. C.-T. Chen, X. Xu, A. Hosseini, Z. Pan, H. Subbaraman, X. Zhang, and R. T. Chen, "Design of highly efficient hybrid Si-Au taper for dielectric strip waveguide to plasmonic slot waveguide mode converter," J. Lightwave Technol. **33**(2), 535–540 (2015).